33RD CONGRESS
OF THE INTERNATIONAL COUNCIL
OF THE AERONAUTICAL SCIENCES
STOCKHOLM, SWEDEN, 4-9 SEPTEMBER, 2022

ICAS 2022 SWEDEN

FLIGHT TESTS AND SIMULATION OF A HANG GLIDER

Taichi Takamatsu[1] and Yoshimasa Ochi[2]

[1]National Defense Academy, Yokosuka, Kanagawa, 239-8686, Japan; email: taichi.19831220@gmail.com
[2]National Defense Academy, Yokosuka, Kanagawa, 239-8686, Japan; email: ochi@nda.ac.jp

Abstract

This paper describes the flight data measurement system developed and shows flight test results obtained using a hang glider, Wills Wing Sport 2. The measurement system comprises three subsystems: the inertial measurement system, the force measurement system, and the image capturing system. Five flights with four patterns of maneuver for each flight were done. This paper shows the results of the pitching and right turn maneuvers, compared with simulation results computed using a dynamic model we had proposed for another hang glider.

Keywords: flight test, simulation, modeling, dynamic flight model, flight mechanics

1. Introduction

A hang glider is a lightweight flying-wing-type aircraft with a simple structure. The pilot is suspended from the wing and handles the vehicle by pushing or pulling the triangular control frame attached to the keel. There are no control surfaces, unlike typical fixed-wing aircraft. Several researchers, including the present authors, studied the flight dynamics of a hang glider and reported its dynamic models, only showing simulation results, using their models, if any [1-5].

Phillips [1] investigated the static longitudinal stability and pilot's longitudinal and lateral control forces for the Rogallo-wing configuration and his proposed straight-wing configuration with control surfaces. de Matteis [2] proposed a dynamic model, considering the pilot's relative rotational motion and defining the pilot's handling force applied to the base bar as the input; however, no consideration was given to the internal force between the wing and the pilot. Cook and Spottiswoode [3] showed linear equations of motion in which the pilot's relative attitude to the wing was defined as the control input; hence, they did not consider the pilot's relative motion. Rogers [4] presented a dynamic model composed of two separate equations of motion for the wing and pilot, where the pilot's control force was assumed to be in proportion to the pilot's relative attitude to the wing and its derivative. Although the present authors' model [5] is also composed of the wing's and pilot's dynamic models, the two models are integrated into a single dynamic model by analytically eliminating the internal force at the hang point and by regarding the pilot's control force as the input, resulting in a nine-degree-of-freedom (9-DoF) dynamic model expressed as a nonlinear state-vector equation. The physical consistency of this model was illustrated through linear analysis using a linearized model and nonlinear simulations, where the pilot's control was modeled by proportional control with the attitude angular rate feedback and proportional-integral (PI) control with the attitude angle feedback.

However, to verify the true effectiveness of the dynamic model, we need to perform flight tests and identify the model's parameters, conduct simulations using the identified model, and compare the results with flight test data. For this purpose, we developed a flight measurement system for a hang glider and conducted flight tests. This paper describes the measurement system and presents flight test and simulation results to verify the qualitative validity of our proposed model.

This paper is organized as follows. In Section 2, the outline of the 9-DoF dynamic model is shown along with the definition of the variables. Section 3 presents the flight measurement system, followed by Sections 4 and 5 to show flight test and simulation results. Finally, conclusions are given in Section 6.

2. 9-DoF Nonlinear Dynamic Model

Figure 1 shows the configuration of a hang glider and the definition of the wing- and pilot-fixed coordinate systems: $\Sigma_w(X_w, Y_w, Z_w)$ and $\Sigma_p(X_p, Y_p, Z_p)$, respectively. The origins of Σ_w and Σ_p are the center of gravity (CG) of the wing and pilot, respectively. The X_w-axis of the wing is along the keel, the Z_w-axis is taken to be vertically downward in the symmetry plane of the wing, and the Y_w-axis is defined to form the right-hand system. The X_p-axis of the pilot is along the pilot's body centerline, the Z_p-axis is taken vertically downward in the symmetry plane of the pilot, and the Y_p-axis is defined to form the right-hand system.

The dynamic model is given in the form of a state-vector equation by

$$\dot{x} = f(x) + g(x)u \tag{1}$$

where $x = [u_w\ v_w\ w_w\ p_w\ q_w\ w_w\ p_{pw}\ q_{pw}\ r_{pw}\ \phi_{pw}\ \theta_{pw}\ \psi_{pw}\ \phi_w\ \theta_w\ \psi_w]^T$ is the state vector, $u = [T_{cx}\ T_{cy}\ T_{cz}\ T_{dx}\ T_{dz}]^T$ is the input vector. The state and control variables are defined as follows. u_w, v_w, and w_w: the velocity components of the wing; p_w, q_w, and r_w: the angular velocity components of the wing; p_{pw}, q_{pw}, and r_{pw}: the pilot's angular velocity components relative to the wing; ϕ_{pw}, θ_{pw}, and ψ_{pw}: respectively the pilot's roll, pitch, and yaw angles relative to the wing; ϕ_w, θ_w, and ψ_w: respectively the wing's roll, pitch, and yaw angles, where the attitude angles are defined as Euler angles; T_{cx}, T_{cy}, and T_{cz}: the X_w-, Y_w-, and Z_w-components of the sum of the pilot's right- and left-hand control forces applied on the base bar; T_{dx} and T_{dz}: the X_w- and Z_w-components of the difference between the pilot's right- and left-hand control forces applied on the base bar.

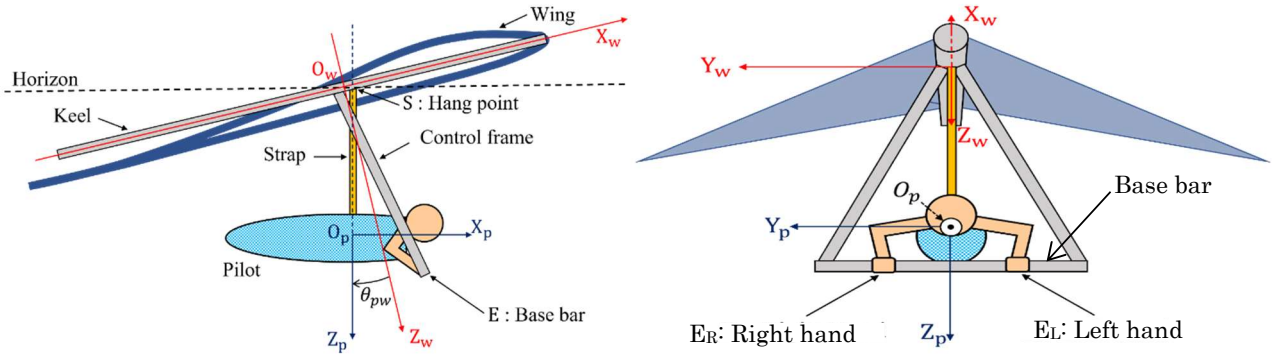

Figure 1 – Configuration of a hang glider and definition of the coordinate systems. (left: sideview, right: front view)

3. Flight Measurement System

In order to measure the state and control variables, we developed a flight measurement system using two inertial measurement units (IMUs) with GPS receivers and two force sensors, which is composed of three measurement subsystems with a suite of these sensors: inertial measurement subsystem, force measurement subsystem, and image capturing subsystem, as shown in Figure 2.

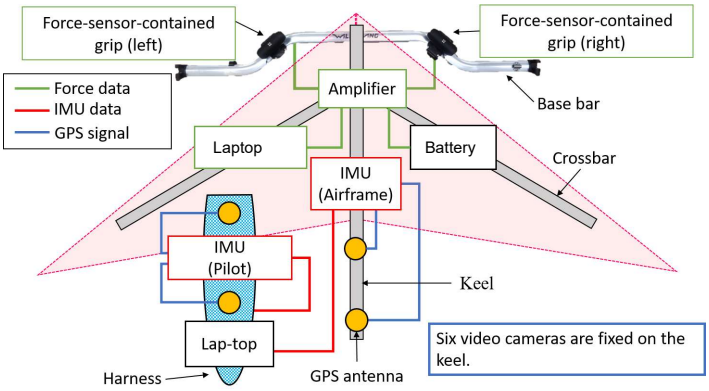

Figure 2 – Architecture of the flight measurement system (top view).

3.1 Inertial Measurement Subsystem

The inertial measurement subsystem comprises two IMUs with GPS antennas (VectorNav, VN-300) and a laptop computer, as shown in Figure 3. One IMU is mounted at the airframe's CG position under the keel, and its two GPS antennas are placed on the rear part of the keel. The other IMU, along with its GPS antennas, is fixed on an acrylic resin plate, which is put inside the back pocket of the harness to measure the pilot's motion. The measurements of the IMUs are recorded in the laptop contained in the harness's side pocket. Although the harness is flexible, the plate is fixed in the back pocket so that the IMU on the pilot measures the pilot's motion as a rigid body.

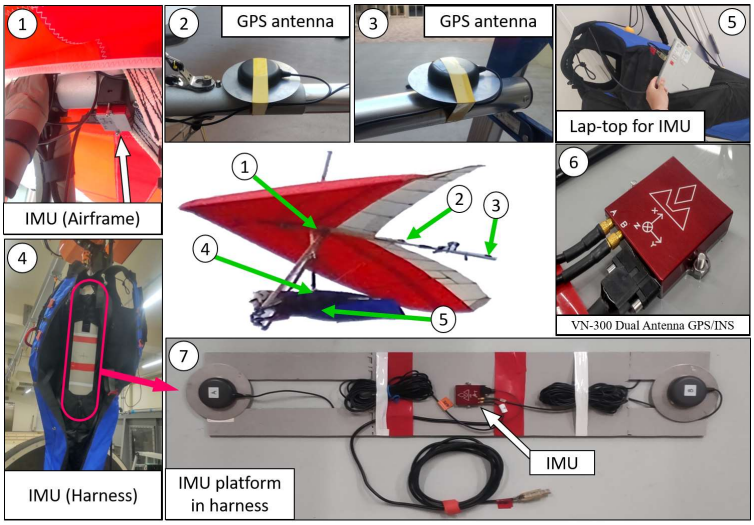

Figure 3 – Inertial measurement subsystem.

3.2 Force Measurement Subsystem

The force measurement subsystem comprises the right and left grips containing a 3-axes force sensor. The grips installed on the base bar are carefully designed so that the pilot feels as if he/she gripped the base bar directly. The measurements are transmitted to a laptop through an amplifier and recorded. The laptop and amplifier are fixed on the keel and right-wing crossbar, respectively, and the battery is on the left-wing crossbar.

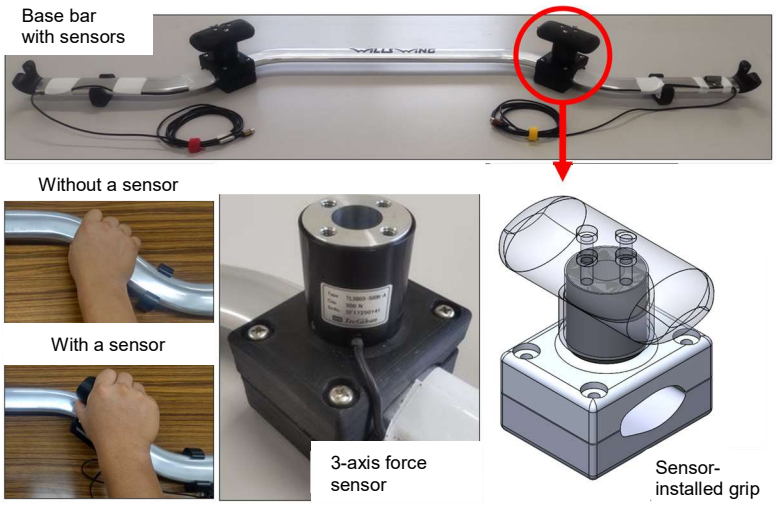

Figure 4 – Inertial measurement subsystem.

3.3 Image Capturing Subsystem

The image capturing subsystem takes videos of the pilot and wing tips with six digital video cameras placed on the keel. The camera placement and the pictures taken from each camera are shown in Figure 5. Although the cameras were originally intended to provide images for motion analysis, we gave up using them for this purpose because it was found to be difficult to track the orange markers on the back of the harness. However, the images obtained helped us understand the motion and handling of the pilot.

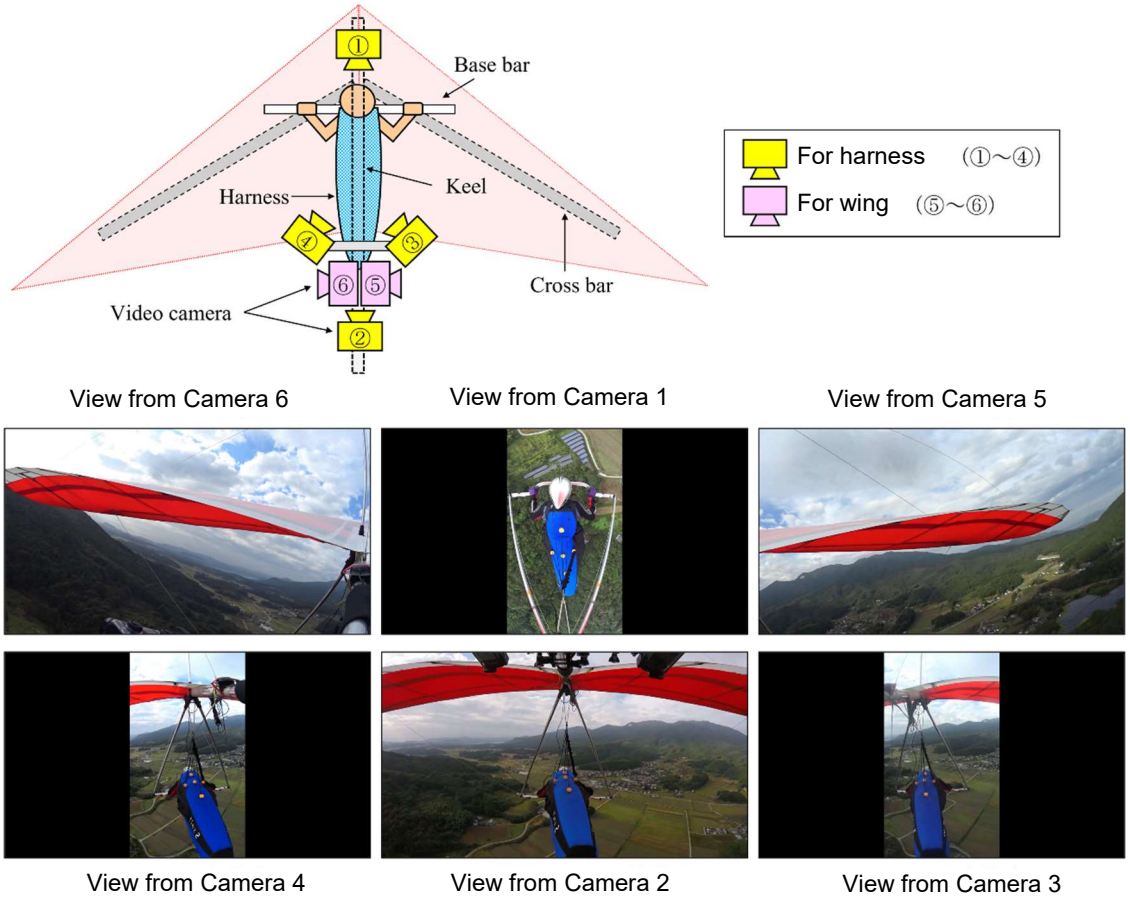

Figure 5 – Image capturing subsystem and images taken by the cameras.

4. Flight Test

4.1 Flight Test Conditions and Procedure

We conducted flight tests using a Wills Wing Sport 2, model 155. The configuration characteristics are shown in Table 1.

Table 1 Configuration characteristics

Wing type	Double surface
Wing area	14.4 m^2
Wing span	9.60 m^2
Aspect ratio	6.40
Airframe weight	26.8 kg
Airframe length	5.08 m
Permitted payload weight	68 – 113 kg
Recommended pilot weight	60 – 80 kg

Flight tests were conducted in the early morning on August 27 and October 27, 2021, in the Itajiki Mountain flight area for hang gliders in Ishioka, a city about 80 km north of Tokyo. Two flights were done on August 27 and three flights on October 27. The altitude of the take-off and landing points is 335 m and 49 m, respectively. The weather was clear or partly clouded, and the wind was calm at take-off. On any flight, the flight time was about 4 min. The weight of the wing, including the measurement units, is 33.4 kg and that of the pilot, including the harness and measurement units, is 72.6 kg. The flight patterns are as follows:

Case 1: Steady straight gliding

Case 2: Pitching maneuver

Case 3: Steady left turn

Case 4: Steady right turn

In each flight, the pilot sequentially performed the maneuver from Case 1 to Case 4.

To synchronize the measurements of the IMU and the force sensors recorded by different laptops, the pilot lifted the airframe a little and dropped it just before take-off. The recorded acceleration and force measurement spikes allowed us to synchronize the sensors' data. The pilot also tapped the grips at the test cases' start and end times to identify each case. This pilot's action allowed us to synchronize the video images and the sensor measurements.

4.2 Flight Test Results

The flight data were cut out for each test case using the spikes. Out of the 20 test cases, we show the results in Case 2 of the second flight and Case 4 of the first flight on October 27.

4.2.1 Pitching Maneuver (Case 2)

Figure 6 shows time histories of the pilot's control forces on the base bar, wing attitudes, body-axis ground speeds, and body-axis accelerations in Case 2, respectively. In the pitching motion, as seen from the time response of the pilot's force along the X_w-axis, T_{cx}, in Figure 6-a, the pilot repeated pulling the base bar and releasing the force three or four times, resulting in the motion of pitch-up and pitch-down, as shown in Figure 6-b. During the pitching motion, although the yaw angle changes about 30 deg, the roll angle variation of the wing is within ±3 deg, which is achieved by the pilot's lateral control to keep the flight path straight, as seen from T_{cy} in Figure 6-a. In Accordance with the pitching motion, the X_w-axis ground speed of the wing, u_w, in Figure 6-c varies as large as 2.5 m/s in amplitude, whereas the Z_w-axis speed, w_w, varies within the range of 0.8 m/s.

The pilot's pitch angle is smaller than the wing's by 5 to 15 deg. The difference decreases when the pilot pulls the base bar and increases when releasing the pulling force. The wing's pitch angle changes, but the pilot's longitudinal attitude stays around the level. There are two reasons for this. One is that the pilot is suspended by the hang strap and freely swings about the hang point. The other is that the pilot is about two times heavier than the airframe, which causes the pilot to change the pitch angle less than the wing. From the time responses of the forward speed and the pitch angle, we see that by pulling the base bar, the wing pitches down and the forward speed increases, and then the pitch angle begins to increase, and the forward speed decreases. This wing's motion indicates longitudinal static or speed stability. The pilot should feel the pulling or pushing force for pitching as the so-called 'bar pressure.'

4.2.2 Right Turn (Case 4)

Figure 7 shows the results of the right turn. To start the maneuver, the pilot pushes the base bar to the left, as seen from the negative T_{cy} from about 2.5 s through 11 s in Figure 7-a, and to return to the straight glide, he/she pushes the bar to the right after 27 s. Figure 7-b shows that the wing rolls approximately by 30 deg in 7 s. From 12 s through 27 s, the roll angle stays at about 33 deg, indicating the steady right turn; accordingly, the yaw angle increases by about 700 deg, which corresponds to two turns, in which, as seen from Figure 7-c, the ground speed increases by about two m/s due to the roll and pitch down.

While increasing the roll angle, the pilot's roll angle is 2 or 3 deg smaller than the wing's because the pilot pushes the bar to the left and moves to the right from the center of the base bar. On the other hand, while decreasing, the pilot's roll angle is larger because he/she pushes the bar to the right.

During the steady turn, the pilot's roll angle is slightly smaller than the wing's, which indicates that the centrifugal force to roll the pilot is balanced with force due to the gravity, resulting in the pilot's position almost in the symmetry plane or the X_wZ_w-plane. Note that the small inverse response of the roll angle at 3 s and 28 s is observed, although the latter is not so evident. This response is caused by the reaction of the pilot's pushing the base bar. The inverse response at 28 s is minor, probably because of the pilot's slowly increasing sideward force T_{cy} compared with the fast one at 3 s. The pitch angle between the wing and the pilot decreases during the turn due to the wing's pitch down. While rolling into the bank, T_{cx} is negative, but T_{cz} is positive, which means that the pilot pulls backward and pushes downward, whereas, during the rolling out of the bank, both T_{cx} and T_{cz} are negative, indicating that the pilot pulls the bar back and upwards. The positive T_{cz} may be caused to resist the bar pressure due to the pitch-down and speed increase, and the negative may be attributed to the pitch up and speed decrease.

Another remarkable pilot's handling is seen in T_{cx} in Figure 7-a, where the left- and right-hand forces with a large magnitude in the opposite direction are applied while the pilot rolls the wing, as pilots are instructed to do so when rolling. Although T_{cx} does not directly affect the rolling motion, instead, the force makes the pilot's yaw angle perpendicular relative to the base bar to assure the pilot's sideward CG shift, which allows the pilot to apply firmly the sideward force T_{cy} to the base bar, as shown in Figure 7-a. This pilot's action keeps the roll angle more minor than the wing's while rolling into the bank and larger while returning from the bank. We also find that T_{cx} and T_{cy} are less than 10 N during the steady turn, but T_{cz} is about 30 N. We consider this T_{cz} is due to the weight of the pilot's hands.

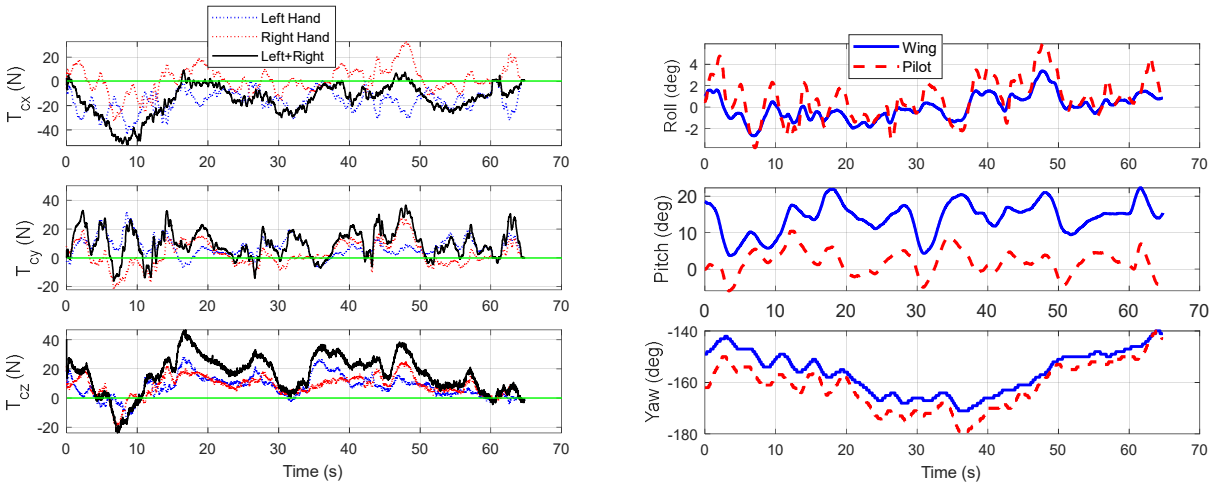

a: Pilot's control forces

b: Attitudes of the wing and pilot

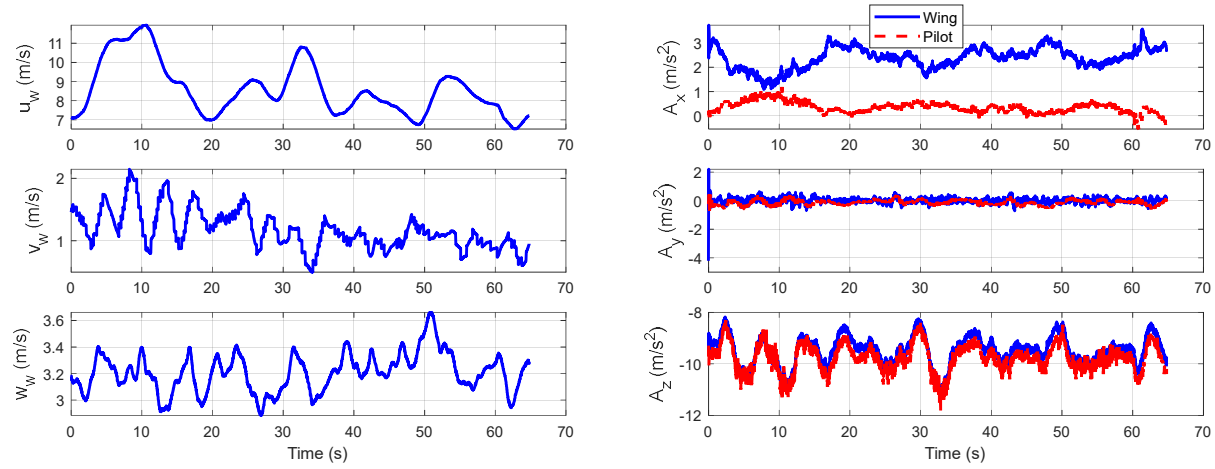

c: Body-fixed-axis speeds of the wing

d: Body-fixed-axis accelerations

Figure 6 – Flight test results of the pitching maneuver (Case 2).

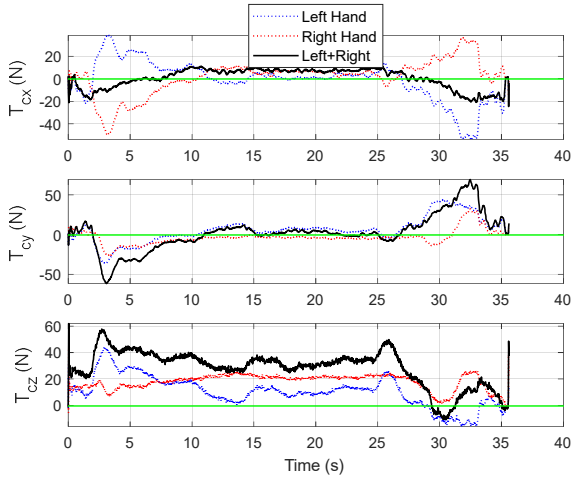

a: Pilot's control forces

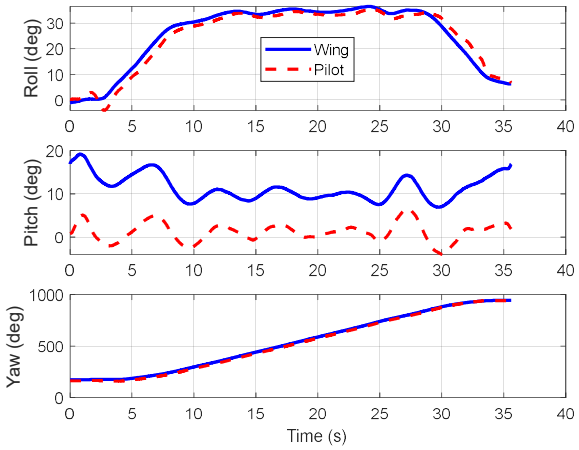

b: Attitudes of the wing and pilot

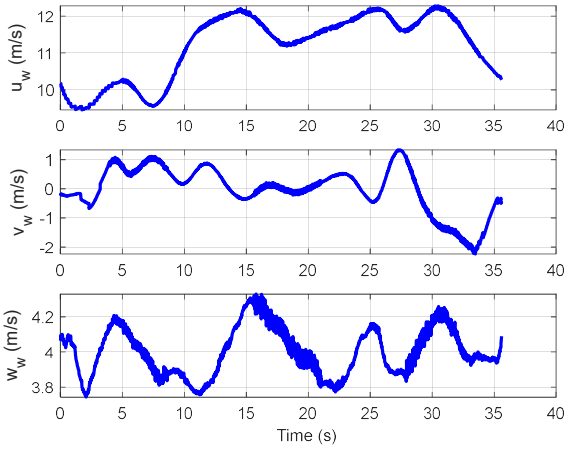

c: Body-fixed-axis speeds of the wing

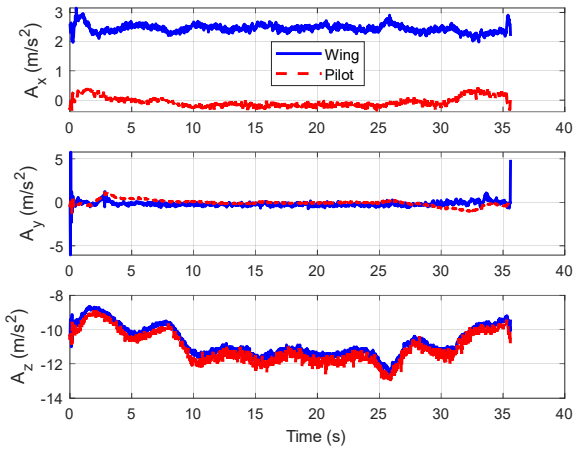

d: Body-fixed-axis accelerations

Figure 7 – Flight test results of the right turn (Case 4).

5. Simulation

We conducted simulations using the dynamic model [5] with the parameters given in [2] for a hang glider, Hiway Demon, which is in a similar class as the one used in the flight tests. In the simulations, the proportional-integral (PI) control gave the pilot's control forces to duplicate the flight test data of the roll and pitch angles. Specifically, the control laws are as follows:

$$\Delta T_{cxp} = K_{P\theta}\tilde{\theta}_w + K_{I\theta}\int_0^t \tilde{\theta}_w d\tau \tag{2}$$

$$\Delta T_{cyp} = K_{P\phi}\tilde{\phi}_w + K_{I\phi}\int_0^t \tilde{\phi}_w d\tau \tag{3}$$

where ΔT_{cxp} and ΔT_{cyp} are deviations from the trim control force T_{cxp}^* and T_{cyp}^* (=0), respectively.; The subscript 'p' indicates that the force is defined in the pilot coordinate system Σ_p.; The symbol '~' denotes the control error, i.e., $\tilde{\theta}_w := \theta_{wc} - \theta_w$ and $\tilde{\phi}_w := \phi_{wc} - \phi_w$, where θ_{wc} and ϕ_{wc} are the reference outputs to θ_{wc} and ϕ_{wc}, respectively. First-order lag systems generate the reference outputs for rectangular command inputs. We determined the control gains, time constants of the first-order systems, and the command inputs by trial-and-error simulation. The pilot's relative yaw angle control mentioned in Section 4.2.2 was also integrated into the pilot's handling as the PI control:

$$\Delta T_{dxp} = K_{P\psi}\tilde{\psi}_{pw} + K_{I\psi}\int_0^t \tilde{\psi}_{pw} d\tau \tag{4}$$

where $\tilde{\psi}_{pw} := \psi_{pwc} - \psi_{pw}$; ψ_{pwc} (=0) the reference output. The pilot's relative motion to the wing is

damped by $\Delta T_{cyp} = K_p p_{pw}$, $\Delta T_{cxp} = K_q q_{pw}$, and $\Delta T_{dxp} = K_r r_{pw}$, which are added to the control inputs given by Eqs. (2), (3), and (4). Since the control forces are defined in the pilot coordinate system Σ_p, they are transformed into the wing coordinate system Σ_w, shown in the figures below.

Figure 8 shows the simulation results for Case 2. Although the roll angle response in the flight test is more fluctuating than that in Figure 8, its magnitude is small. Since the roll and pitch angle controls are not tight enough to track their reference outputs, significant control errors result; the pitch angle response, however, is similar to that in the flight test. The time responses of u_w, A_x, A_y, A_z, and the control force T_{cx} are also well reproduced.

Figure 9 shows the simulation results for Case 4. The roll angle of the wing is similar to that in the flight test. Although the inverse response of the pilot's roll angle around 3 s and 29 s appears, its magnitude is more prominent. Note that the control force T_{cy} is about twice as large as in Figure 7-a. This control force may have resulted in a significant inverse response. The large T_{cy} is that in the simulation, the effect of wires spanned between the base bar and the wing, which will transmit the control force to the wing to increase the moment arm for rolling, is not considered.

The pitch angle response is also similar to that of the flight test. T_{cx} in the opposite directions given by Eq. (4) appears, as in the flight test. However, the magnitude of the right- and left-hand control forces is two or three times larger than those in the flight test. The reason for this will be the high control gain for the pilot's relative yaw angle control.

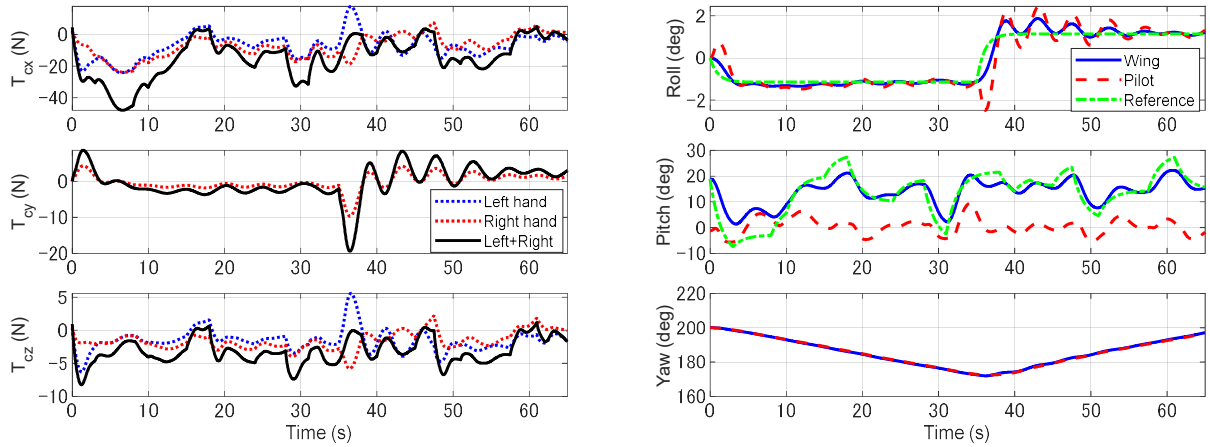

a: Pilot's control forces

b: Attitudes of the wing and pilot

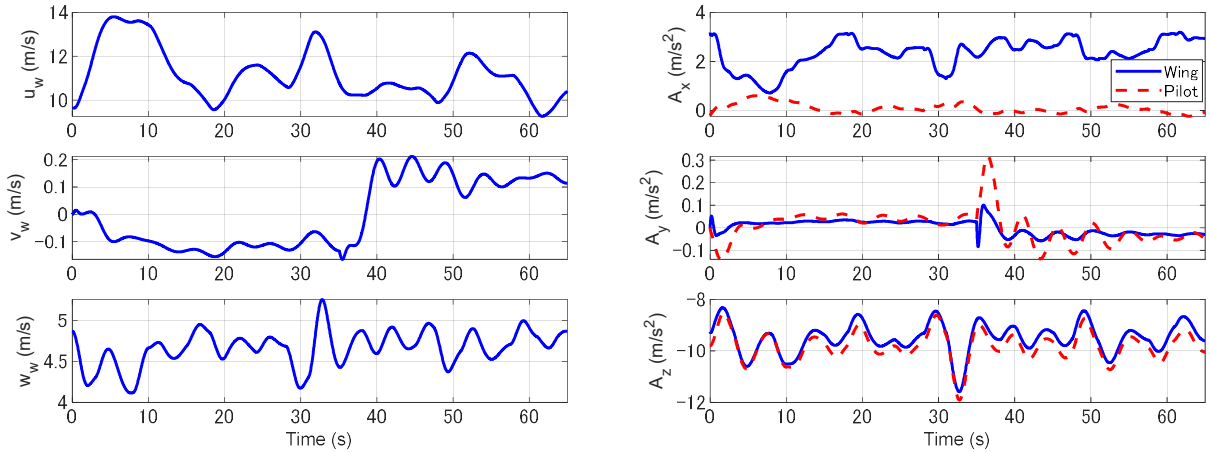

c: Body-fixed-axis speeds of the wing

d: Body-fixed-axis accelerations

Figure 8 – Simulation results of the pitching maneuver (Case 2).

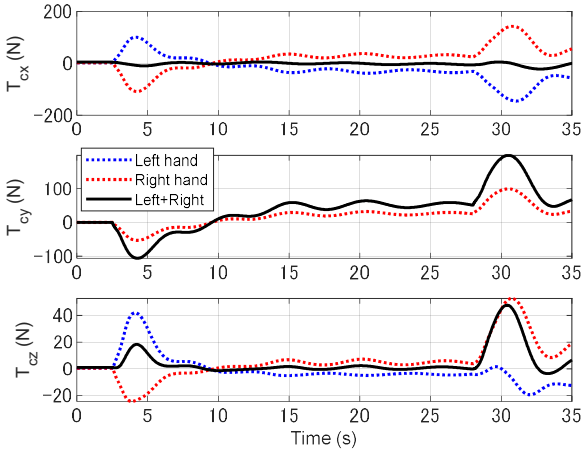

a: Pilot's control forces

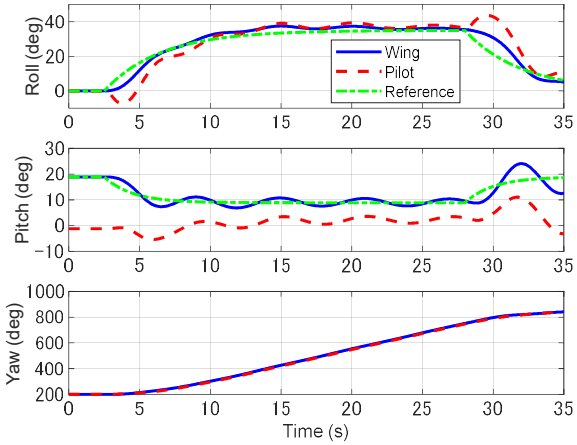

b: Attitudes of the wing and pilot

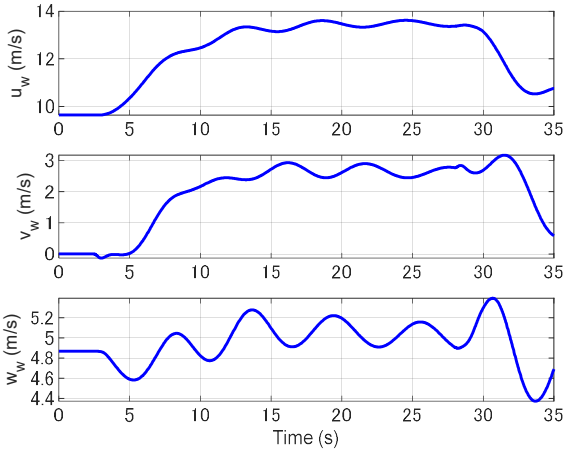

c: Body-fixed-axis speeds of the wing

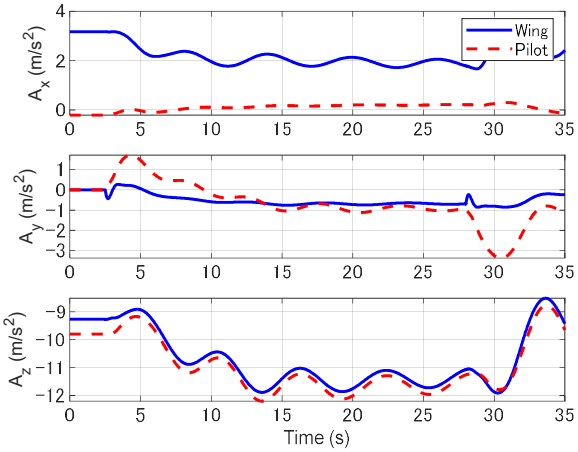

d: Body-fixed-axis accelerations

Figure 9 – Simulation results of the right turn maneuver (Case 4).

Remark: It is said that the hang glider maneuvers by the pilot's CG shift. It would be wrong if this idea came from the analogy of the balance inclining when its CG moves. As the flight test and simulation results show, the hang glider maneuvers by the pilot's pushing or pulling the base bar, which causes the wing to pitch or roll as a reaction since the pilot's weight is more than two times larger than the airframe. Furthermore, note that the strap suspends the pilot from the hang point near the CG, on which most of the pilot's weight is, which means the pilot's weight shift produces little moment. The pilot's shift results from applying the control force and is not a cause for maneuvering. Particularly when turning, by moving sideward and keeping the yaw attitude perpendicular to the base bar, the pilot can continue to apply the sideward force until the steady turn is established.

6. Conclusions

We have described the flight measurement system for a hang glider and presented the flight test results for the pitching and right turn maneuvers, showing the consistent relation between the pilot's control forces and the maneuvers. We also presented the simulations that duplicate the roll and pitch angle responses in the flight tests using the pilot's control force generated by the PI control laws. The simulation results are mostly consistent with the flight test results, suggesting the qualitative validity of the dynamic model of a hang glider proposed by the authors. However, some variables and control inputs differ greatly from the flight tests. We need to modify the model to remove the discrepancies while considering added mass. We are to estimate the moments and products of inertia based on the ground experiments and identify aerodynamic parameters using the flight test data to establish a hang glider's dynamic model.

Acknowledgment

The test pilot is Mr. Yuji Suzuki, a professional hang glider pilot who placed 12th at the 22nd Hang Gliding World Championships in Italy in 2019. The authors would record grateful acknowledgments for his support.

References

[1] Phillips, W. H., Analysis and experimental studies of the control of hang gliders, *Proc. AIAA/MIT/SSA 2nd International Symposium on the Technology and Science of Low Speed and Motorless Flight*, pp 1-12, 1974. (AIAA 74-1030)

[2] de Matteis, G., Dynamics of hang gliders, *AIAA Journal of Guidance, Control, and Dynamics*, Vol. 14, No. 6, pp 1145-1152, 1991.

[3] Cook, M. V. and Spottiswoode, M., Modelling the flight dynamics of the hang glider, *The Aeronautical Journal*, January, pp 1-20, 2006.

[4] Rogers, R. M., Longitudinal dynamics and stability of hang-gliders with pilot control reaction, *Proc. AIAA Atmospheric Flight Mechanics Conference*, pp 1-14, 2007. (AIAA 2007-6307)

[5] Ochi, Y., Modeling of flight dynamics and pilot's handling of a hang glider, *Proc. AIAA Modeling and Simulation Technologies Conference*, pp 1-19, 2017. (AIAA 2017-1758)